Nanometer Linear Focusing of Hard X Rays by a Multilayer Laue Lens

H. C. Kang,[1,2] J. Maser,[1,3,*] G. B. Stephenson,[1,2] C. Liu,[3] R. Conley,[3] A. T. Macrander,[3] and S. Vogt[3]

[1]*Center for Nanoscale Materials, Argonne National Laboratory, Argonne, Illinois 60439, USA*
[2]*Materials Science Division, Argonne National Laboratory, Argonne, Illinois 60439, USA*
[3]*Experimental Facilities Division, Argonne National Laboratory, Argonne, Illinois 60439, USA*

(Received 30 September 2005; published 27 March 2006)

We report on a type of linear zone plate for nanometer-scale focusing of hard x rays, a multilayer Laue lens (MLL), produced by sectioning a multilayer and illuminating it in Laue diffraction geometry. Because of its large optical depth, a MLL spans the diffraction regimes applicable to a thin Fresnel zone plate and a crystal. Coupled wave theory calculations indicate that focusing to 5 nm or smaller with high efficiency should be possible. Partial MLL structures with outermost zone widths as small as 10 nm have been fabricated and tested with 19.5 keV synchrotron radiation. Focal sizes as small as 30 nm with efficiencies up to 44% are measured.

DOI: 10.1103/PhysRevLett.96.127401 PACS numbers: 78.67.Pt, 07.85.Fv, 41.50.+h, 78.70.Ck

Feynmann's dictum that "*There is plenty of room at the bottom*" is being tested lately for focusing of hard x rays ($\lambda < 0.1$ nm). Where that ultimate bottom limit for spatial resolution may lie on the nanometer scale is a question that has caused some considerable discussion and effort in the x-ray physics and x-ray optics communities. The answer is important for the many fields of science that make use of x-ray microprobes and high-resolution x-ray microscopes. Several optics approaches have been explored recently to address the question theoretically [1,2] and to push the limit experimentally [3–8].

The diffraction limit for resolution given by the Rayleigh criterion is $R_{\mathrm{dl}} = 0.5\lambda/\mathrm{NA}$ [9], where NA is the numerical (angular) aperture of the focusing optic. While hard x rays provide small wavelengths λ, the long-standing difficulty has been to achieve a high NA. The interaction of hard x rays with matter is inherently weak, so that efficient deflection of x rays by a single interface occurs only at small angles. Higher NA can be achieved using diffractive optics employing many interfaces, such as Fresnel zone plates. However, there are two main problems: (i) To date it has been difficult to fabricate zone plates having the combination of nm-scale zone widths, required for small focal sizes, and μm-scale depths, needed for high efficiency at hard-x-ray wavelengths; (ii) more fundamentally, the standard flat zone plate geometry has a low efficiency for nm-scale focusing of hard x rays, owing to volume diffraction effects [10].

In this Letter we report calculations and measurements on a new type of linear zone plate, a multilayer Laue lens (MLL), which advances the solutions to both of these problems [11]. As shown in Fig. 1, a MLL is a cross section of a planar multilayer sputtered film, illuminated nearly edge on, so that the layers form Fresnel zones. This allows fabrication of structures with very large zone depth-to-width ratios, and tilting of the structures to improve efficiency. The interfaces within the MLL are positioned according to the binary zone plate law $r_n^2 = n\lambda f + n^2\lambda^2/4$, where r_n is the distance from the nth interface to the optical axis and f is the focal length [12]. Note that the second term is negligible for the cases considered here. The d spacing, $\Lambda(r_n) \equiv r_n - r_{n-2} \approx \lambda f/r_n$, varies inversely with position in the multilayer. The MLL operates in the volume diffraction regime, ranging from multibeam kinematic scattering applicable to a thin Fresnel zone plate, to dynamical diffraction applicable to a crystal. For this reason, calculation of the optical performance of a MLL is nontrivial. Unlike a thin zone plate, its behavior can depend strongly on the angle of the layers with respect to the incident beam. We have modeled the three types of MLL structures shown in Fig. 1. The "flat" case (a), with all layers parallel to the optical axis, is the analogue of a standard x-ray zone plate fabricated by lithography. The "ideal" case (b), with each layer satisfying its Bragg condition $\theta = \theta_B \approx \lambda/2\Lambda$, has best performance but is difficult to fabricate. We also consider the "tilted" case (c), which is an approximation to the ideal case. We have fabricated and measured the performance of partial MLL structures of the tilted type (c).

To model MLL performance we use coupled wave theory in an N-wave representation [10,13,14]. In this approach, local diffraction properties are calculated for each position using a locally constant d spacing and accounting

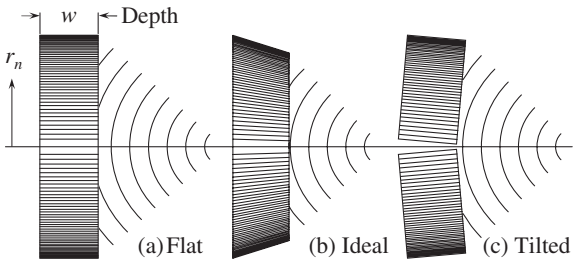

FIG. 1. Schematics of (a) flat MLL (all layers aligned to axis), (b) ideal MLL (each layer at its Bragg angle), and (c) tilted MLL (each half tilted to an average Bragg angle).

for the angle of the layers with respect to the incident beam. The wave field inside the MLL can be described using a Fourier series containing many eigenmodes corresponding to different diffraction orders. At each position r_n, a self-consistent solution for the complex amplitudes of all eigenmodes as a function of location within the MLL depth is obtained by numerically solving the set of coupled differential equations that describe solutions of Maxwell's equations [10]. The diffracted wave front from the entire MLL structure is then constructed from the local complex amplitudes at the exit surface for all r_n [11].

These calculations capture the essential variation of the diffraction behavior of the MLL with r_n [10]. Near the optical axis, where the d spacing Λ is large, the MLL acts as a thin grating, with many diffraction orders excited and little sensitivity to incidence angle. Far away from the axis, where Λ is small, the MLL acts like a dynamically diffracting crystal. Only two orders are excited, and satisfying the Bragg condition is critical to obtaining high efficiency. To adequately describe the wave field inside the MLL at small r_n, while maintaining convergence of the solutions through the depth, we used a total number of 122 eigenmodes. To achieve sufficient local sampling, the MLL is divided into 100 local gratings.

For a structure obeying the zone plate law, diffraction into the 1st order contributes to the primary focus. We plot in Fig. 2 the calculated local efficiency of diffraction into the 1st order as a function of r_n for MLL structures made of WSi_2 and Si layers, with depth $w = 13.5$ μm, at a photon energy of 19.5 keV ($\lambda = 0.064$ nm) [15]. All three cases shown in Fig. 1 are considered, for structures with outermost zone widths $\Delta r_{\min} = 10$ and 2 nm at an outer position of $r_{\max} = 15$ μm ($\Lambda_{\min} = 20$ and 4 nm, $f = 4.72$ and 0.94 mm, respectively). For the tilted cases, the fixed tilt angle was chosen to make the Bragg condition at $r_n =$ 11.25 μm ($\theta = 1.19$ and 5.96 mrad, respectively). All optics show thin-grating behavior at $r_n = 0$; the local efficiency is 0.23 for this binary materials combination and depth, independent of layer tilt angle or $\Delta r_{\min}$ [12]. From the curves for $\Delta r_{\min} = 10$ nm, one can see that the position region near 10 μm corresponds to the transition between thin grating and dynamical diffraction. The flat case loses efficiency at positions above this region, while the local efficiency of the ideal case climbs to 0.67. The tilted case approximates the ideal case, with a somewhat lower efficiency only in the outermost region. In comparison, the transition region for $\Delta r_{\min} = 2$ nm occurs near $r_n = 2$ μm, with the same changes in the efficiencies of the flat and ideal cases. The tilted case, however, does not approximate the ideal case, having high efficiency only in the narrow region near $r_n = 11.25$ μm (and in the thin-grating region near $r_n = 0$). Thus as $\Delta r_{\min}$ becomes smaller, matching the Bragg angle for each position is required to obtain high efficiency. The need for tilting to match θ_B can be related to the large optical depth w of the MLL. It occurs for $\Delta r_{\min}$ smaller than $\sim 0.5(\lambda w)^{1/2}$ [16], which is 15 nm for the present case.

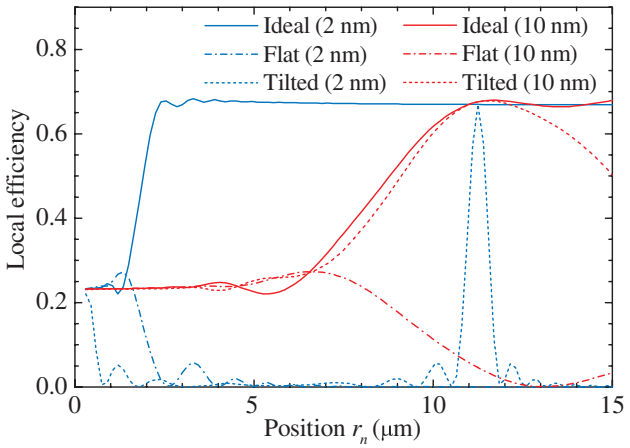

FIG. 2 (color). Calculated local 1st order diffraction efficiency of ideal, flat, and tilted MLL vs position r_n for outermost zone widths $\Delta r_{\min}$ of 2 nm (blue) and 10 nm (red). The optical depth is 13.5 μm, chosen to maximize the integrated efficiency for the ideal case with $\Delta r_{\min} = 10$ nm.

The integrated 1st order efficiency and the spatial resolution calculated for each of the three cases is shown in Fig. 3, as a function of outermost zone width $\Delta r_{\min}$, using the same parameters as in Fig. 2. The integrated efficiency was obtained by averaging the local efficiency over the full aperture of the optic. To obtain the spatial resolution, we first calculate the complex pupil function for the

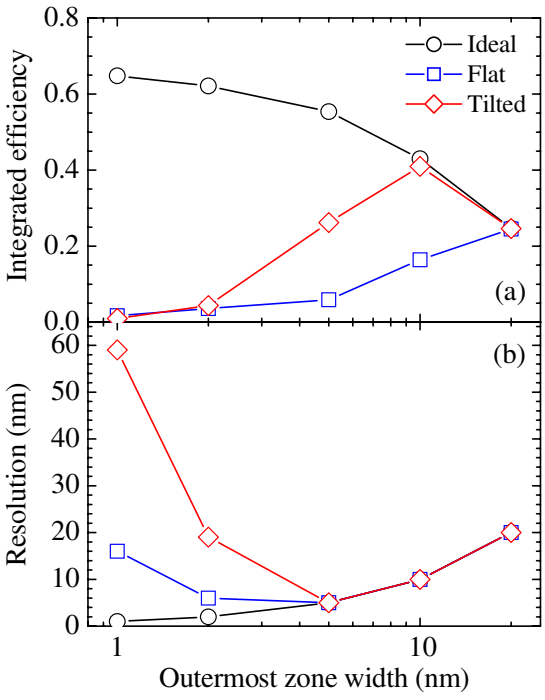

FIG. 3 (color online). Calculated integrated 1st order diffraction efficiency and spatial resolution for ideal, flat, and tilted MLLs vs outermost zone width $\Delta r_{\min}$.

1st diffraction order from the local complex amplitudes at the exit surface [11]. The intensity distribution in the plane of best focus is obtained by multiplying the complex pupil function by a phase factor varied to find the optimal focal length, and taking the Fourier transform of the autocorrelation of this quantity [17]. The resolution plotted in Fig. 3 is the width of the region containing 77% of the intensity, which corresponds to the Rayleigh criterion for a line focus. Calculations were performed for MLL structures with $\Delta r_{\min} = 1$, 2, 5, 10, and 20 nm at $r_{\max} = 15$ μm. One can see that the integrated efficiency of the ideal case increases significantly above the thin-grating value as $\Delta r_{\min}$ is decreased below 20 nm, owing to dynamical diffraction effects. The flat case, on the other hand, shows a significant decrease in efficiency. The tilted case shows improved efficiency over the flat case for $\Delta r_{\min} = 5$ and 10 nm. The calculated spatial resolution of the ideal MLL corresponds to the diffraction limit for a full linear zone plate, $R_{\mathrm{dl}} = \Delta r_{\min}$. The resolutions of both the flat and tilted cases are diffraction limited down to $\Delta r_{\min} = 5$ nm, but then show significant deviations at smaller zone widths. The degradation results from destructive interference caused by phase shifts due to deviations from the Bragg condition [11]. These calculations indicate that a resolution of 5 nm with high efficiency for hard x rays should be possible using the tilted MLL geometry.

To experimentally test these predictions, we have fabricated and characterized partial MLL structures in the tilted geometry. Since the NA of these partial structures is only a fraction of that of a full MLL structure, the best possible resolution R_{dl} is correspondingly larger. Nevertheless, they provide an initial test of MLL performance for the important outer zone region. Three WSi_2/Si multilayers with layer positions following the zone plate law were deposited using dc magnetron sputtering at the Advanced Photon Source (APS). Unlike the previously reported process for ''sputtered-sliced'' zone plates deposited on circular wire cores [18,19], in our case the critical outermost zones are deposited first onto a flat Si substrate [20]. Deposition began with zone $n_{\max}$, and ended before reaching the thickest central zones. As shown in Table I, we deposited somewhat less than half of a full zone plate structure, which for all three cases would have had a thickness of $2r_{\max} = 30$ μm. In addition, electron microscopy of cross sections revealed imperfections in multilayers A and B due to momentary instabilities in the deposition process [20], so that only a part t_{eff} of the total deposited thickness t_{dep} could be used for focusing. Multilayers were sectioned and polished to the final depths w as described previously [21].

Synchrotron x-ray measurements reported here were performed at APS beam line 12BM, with supporting measurements at beam line 8ID. The incident beam was defined by slits to illuminate the thin-zone region of thickness t_{eff} on one side of the optical axis. A Si(111) monochromator was used to select an x-ray energy of 19.5 keV ($\lambda = 0.064$ nm). Fluorescence from a 10-nm-thick Pt film cross section illuminated edge on was used to measure the intensity distribution at the focus. The far-field diffraction pattern was also measured. The depths w determined from transverse fringe spacing [16] and the tilt angles used are listed in Table I.

We plot in Fig. 4(a) the measured intensity distributions at the focus for each sample, and list in Table I the full width at half maximum (FWHM) R_{meas} determined from Gaussian fits. It is fair to compare the FWHM of a Gaussian fit to R_{dl} since it includes 76% of the intensity. We also list $R_{\mathrm{dl}} = \Delta r_{\min}/p$ for the partial MLL structures, where the fraction of the full zone plate structure is $p = 0.27$, 0.23, and 0.41 for samples A, B, and C, respectively. The measured resolution values are only 25%–35% larger than the diffraction limit, consistent with our theoretical analysis and indicating that MLL structures of high perfection can be fabricated.

The far-field diffraction pattern for sample C is shown in Fig. 4(b). The broad peak between $Q_z = 0.014$ and 0.030 $\mathrm{\AA}^{-1}$ is the 1st order diffraction peak from the MLL. Since there is a linear relation between wave number and position in the MLL, $Q_z = 2\pi/\Lambda = 2\pi r_n/\lambda f$, the diffraction pattern can be loosely interpreted as a measurement of the local efficiency as a function of r_n. The extent of the 1st order peak corresponds to a high efficiency for r_n from 6.7 to 14.3 μm, which is in reasonable agreement with the calculation in Fig. 2. The measured values of integrated efficiency listed in Table I were determined by dividing the integrated intensity of this peak by that of the incident beam. While these values are not directly comparable to the calculations in Fig. 3 because of differences in w, p, and uncertainty in actual layer densities, the high measured efficiencies agree qualitatively with our predictions. Indeed, the 44% efficiency measured for sample C exceeds the maximum possible (40%) from binary thin-

TABLE I. MLL parameters and measured performance for samples A, B, and C.

Sample	$\Delta r_{\min}$ (nm)	Focal length f (mm@19.5 keV)	Deposited zones $n_{\max} - n_{\min}$	t_{dep} (μm)	t_{eff} (μm)	Depth w (μm)	Tilt (mrad)	R_{dl} (nm)	R_{meas} (nm)	Efficiency
A	15	7.08	500 − 31	11.3	8	19.3	1.05	56.3	72.7	0.39
B	10	4.72	750 − 23	12.4	7	18.3	1.31	42.9	57.4	0.24
C	10	4.72	750 − 23	12.4	12.4	18.6	0.97	24.2	30.6	0.44

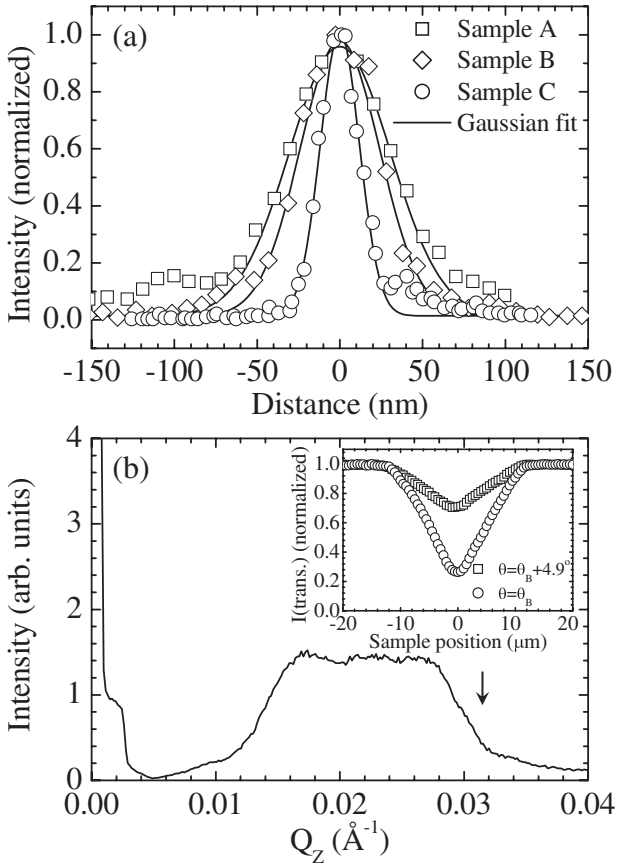

FIG. 4. (a) Measured focal line profiles for samples A, B, and C. The solid lines are Gaussian fits. (b) Far-field diffraction profile of sample C. The Q_z value corresponding to the outermost zone ($r_n = 15$ μm) is indicated by an arrow. Inset: transmission vs sample position at $\theta = \theta_B$ and $\theta \gg \theta_B$.

grating theory [12], demonstrating that volume diffraction effects occur and can be exploited to enhance performance. Another measure of the high diffraction efficiency is indicated in the inset of Fig. 4(b), which shows the dip in the intensity of the zero-order (transmitted) beam when the MLL is scanned through the beam, for two tilt angles. When the tilt angle is far from any Bragg condition, the dip corresponds to absorption only; when the tilt is aligned for 1st order diffraction, the much deeper dip corresponds to absorption plus extinction due to diffraction. Unlike a thin grating, for the MLL, most of the diffracted intensity goes into the 1st order, giving a high focusing efficiency [16].

The measured performance of these partial MLL structures supports the promising theoretical predictions of high-efficiency, diffraction-limited focusing of hard x rays. Although section depth and tilt angle were partially optimized for the measurements presented here, further optimization could yield even higher efficiencies and better resolution. The high efficiencies should make it practical to produce a point focus using 2 MLL's in a crossed configuration [11]. Efficiency is predicted to increase further at higher x-ray energies, as absorption losses decrease. Fabrication of zones by multilayer deposition will allow zone widths smaller than 1 nm, although the challenge will be the accurate placement of the resulting thousands of layers. A periodic transmission multilayer with more than 4000 layers of 3.5 nm thickness has already been demonstrated [16]. The relatively easily fabricated tilted MLL should be adequate to produce 5 nm focal sizes from a full structure. Development of methods to fabricate the ideal MLL geometry should allow focal sizes to approach 1 nm or smaller. The theoretical approach used here finds that the resolution for this ideal case follows the diffraction limit as $\Delta r_{\min}$ decreases, with no bottom limit. We expect that further development of theory will be required, however, to accurately model the behavior of MLL optics for focusing of hard x rays to below 1 nm.

We would like to thank the APS staff at sectors 12 and 8 for capable assistance. Work supported by the U.S. Department of Energy, Office of Science (BES) under Contract No. W-31-109-ENG-38. H. C. K. also acknowledges support from KOSEF.

*To whom correspondence should be addressed.
Electronic address: maser@aps.anl.gov

[1] C. Bergemann, H. Keymeulen, and J. F. van der Veen, Phys. Rev. Lett. **91**, 204801 (2003).
[2] C. G. Schroer and B. Lengeler, Phys. Rev. Lett. **94**, 054802 (2005).
[3] A. Jarre *et al.*, Phys. Rev. Lett. **94**, 074801 (2005).
[4] O. Hignette *et al.*, Rev. Sci. Instrum. **76**, 063709 (2005).
[5] H. Yumoto *et al.*, Rev. Sci. Instrum. **76**, 063708 (2005).
[6] W. Liu *et al.*, Rev. Sci. Instrum. **76**, 113701 (2005).
[7] C. G. Schroer *et al.*, Appl. Phys. Lett. **87**, 124103 (2005).
[8] W. Chao *et al.*, Nature (London) **435**, 1210 (2005).
[9] See, e.g., M. Born and E. Wolf, *Principles of Optics* (Pergamon, New York, 1980), 6th ed. The factor of 0.5 (0.61) applies to a linear (circular) focus.
[10] J. Maser and G. Schmahl, Opt. Commun. **89**, 355 (1992).
[11] J. Maser *et al.*, Proc. SPIE-Int. Soc. Opt. Eng. **5539**, 185 (2004).
[12] J. Kirz, J. Opt. Soc. Am. **64**, 301 (1974).
[13] L. Solymar and D. J. Cooke, *Volume Holography and Volume Gratings* (Academic, New York, 1981).
[14] R. R. A. Syms, *Practical Volume Holography* (Clarendon, Oxford, 1990).
[15] The structure modeled had alternating WSi_2 and Si layers with uniform densities of 9.40 and 2.33 g/cm^3, respectively, and abrupt interfaces.
[16] H. C. Kang *et al.*, Appl. Phys. Lett. **86**, 151109 (2005).
[17] J. W. Goodman, *Introduction to Fourier Optics* (Roberts & Co., Greenwood Village, 2005), 3rd ed.
[18] R. M. Bionta, K. M. Skulina, and J. Weinberg, Appl. Phys. Lett. **64**, 945 (1994).
[19] N. Kamijo *et al.*, Rev. Sci. Instrum. **74**, 5101 (2003).
[20] C. Liu *et al.*, J. Appl. Phys. **98**, 113519 (2005).
[21] H. C. Kang *et al.*, Proc. SPIE-Int. Soc. Opt. Eng. **5537**, 127 (2004).